nature geoscience
SUPPLEMENTARY INFORMATION
DOI: 10.1038/NGEO2974
In the format provided by the authors and unedited.

Abrupt North Atlantic circulation changes in response to gradual CO_2 forcing in a glacial climate state

Xu Zhang[1,2]*, Gregor Knorr[1,3], Gerrit Lohmann[1,4], Stephen Barker[3]

[1]Alfred Wegener Institute Helmholtz Centre for Polar and Marine Research,

Bussestr. 24, D-27570, Germany

[2]Laboratory for Marine Geology, Qingdao National Laboratory for Marine Science and Technology, China

[3]School of Earth and Ocean Sciences, Cardiff University, Cardiff, UK

[4]University of Bremen, Bremen, Germany

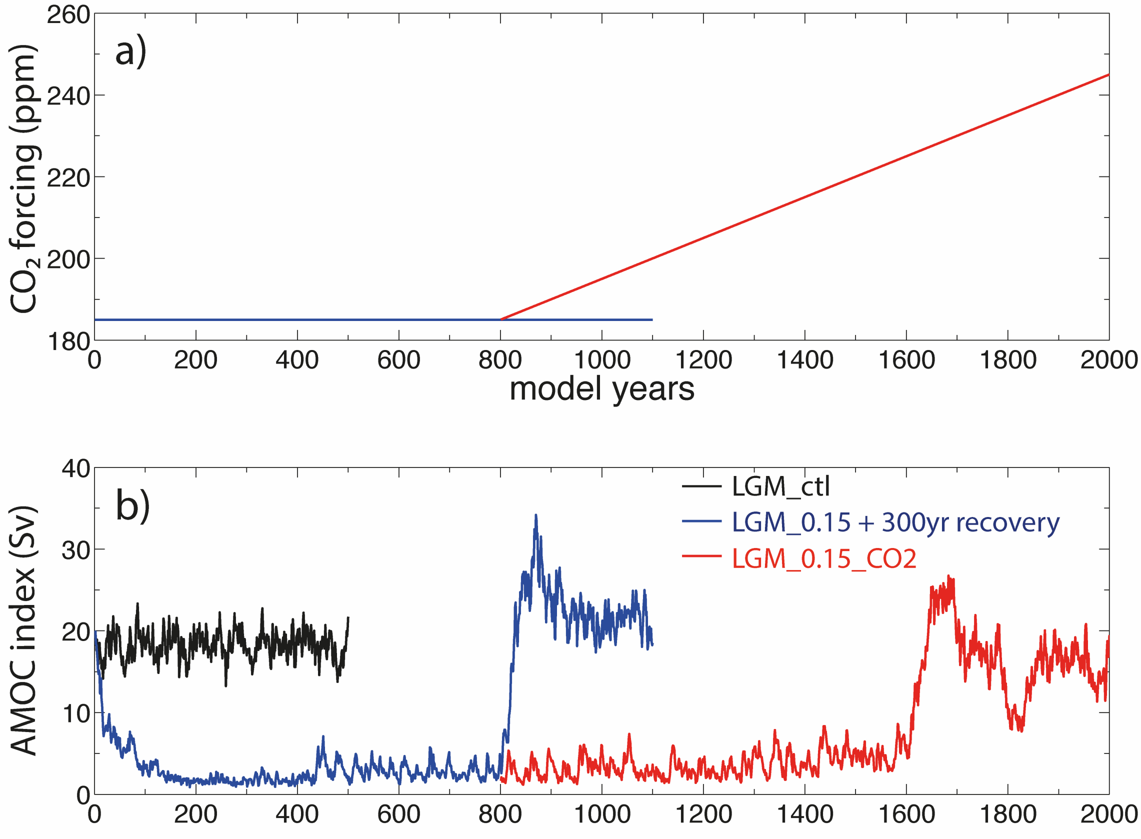

Figure S1 Control simulation (LGM_0.15) of the experiment LGM_0.15_CO2. (a) the CO_2 forcing (ppm), **(b)** the AMOC indices (Sv) of LGM experiment [Zhang et al 2013][9] (blacked line), 0.15Sv NA-hosing experiment (blue line), and the increasing CO_2 scenario of experiment LGM_0.15_CO2 (red line). The perturbation is shut down in the hosing experiment after 801st model years, while the hosing continues all through the experiment LGM_0.15_CO2 as a background climate to mimic the sea level rise.

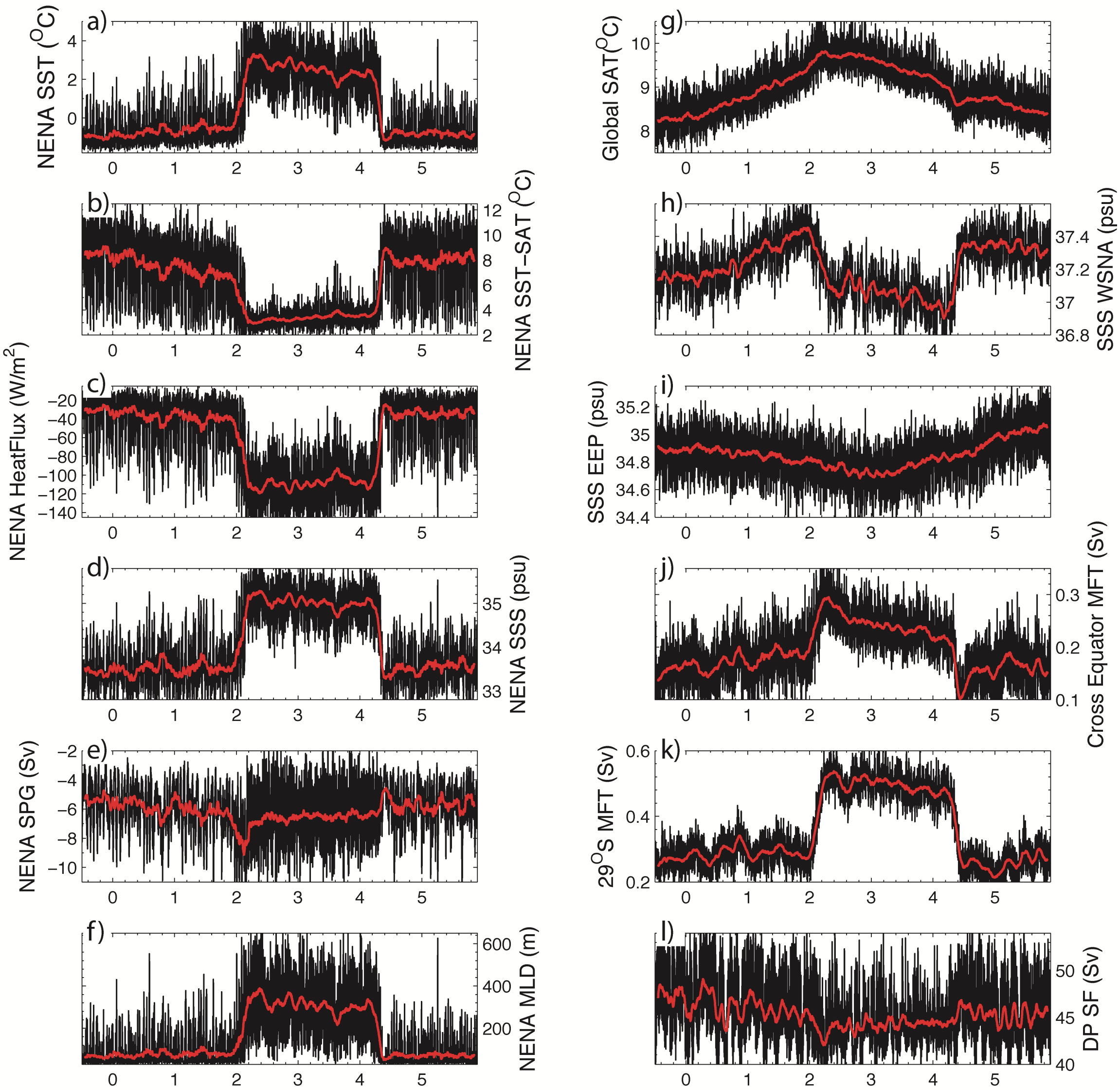

Figure S2 Time series of climate variables in CO2_Hys. (a-f) The indices of sea surface temperature (°C), air-sea surface temperature contrast (°C), surface heat flux (W/m2, the negative represents ocean heat loss), sea surface salinity (psu), Subpolar Gyre strength (Sv) and mixed layer depth (m) over the NENA; (g) global SAT index (°C), (h) sea surface salinity index over the WSNA (psu), (i) sea surface salinity index over the EEP (psu), (j) the MFT (Sv) across the Atlantic equator, (k) the MFT (Sv) across the southern boundary of Atlantic catchment (29°S), (l) barotropic stream function (Sv) across Drake Passage. X-axis (model years, units: kyr) is same as in Fig. 1a-g, i.e. negative model years indicate the control simulations and the positive represents the experiment CO2_Hys. It is proposed that climate variabilities from Southern Hemisphere have the potential of triggering the AMOC recovery from a sluggish AMOC state, e.g. salt import across the southern boundary of the Atlantic catchment (29°S)[31,32] and Drake Passage effect[54]. In addition to a weakened Drake Passage effect in the interval A-B of the weak AMOC mode (l), the experiment CO2_Hys is also characterized by an increased freshwater import across 29°S as the CO2 increases, as shown in k). This indicates climate variability from Southern Hemisphere is of minor importance on triggering the abrupt AMOC transitions. In combination with the increased MFT across the equatorial Atlantic Ocean (j), this evidence further suggests that alterations of tropical water vapor export[55] and the meridional freshwater transport (MFT) in the North Atlantic Ocean are of particular importance[30] on stimulating the AMOC recovery.

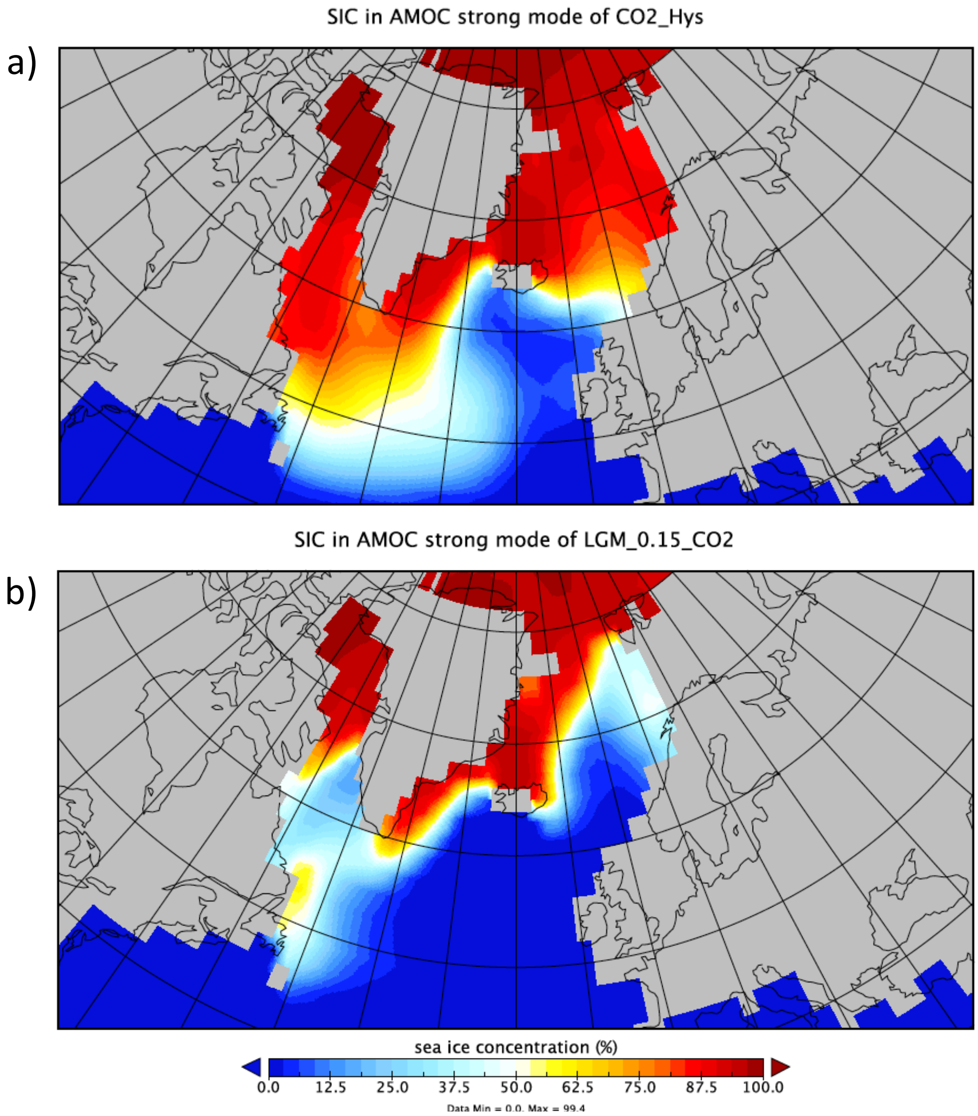

Figure S3 Climatology annual mean sea-ice concentration in the strong AMOC state of experiment CO2_Hys (a) and LGM_0.15_CO2 (b). The strong AMOC states are defined as climatology mean of AMOC peak phases just after AMOC recovery in the warming scenarios of CO2_Hys and LGM_0.15_CO2. units: percentage.

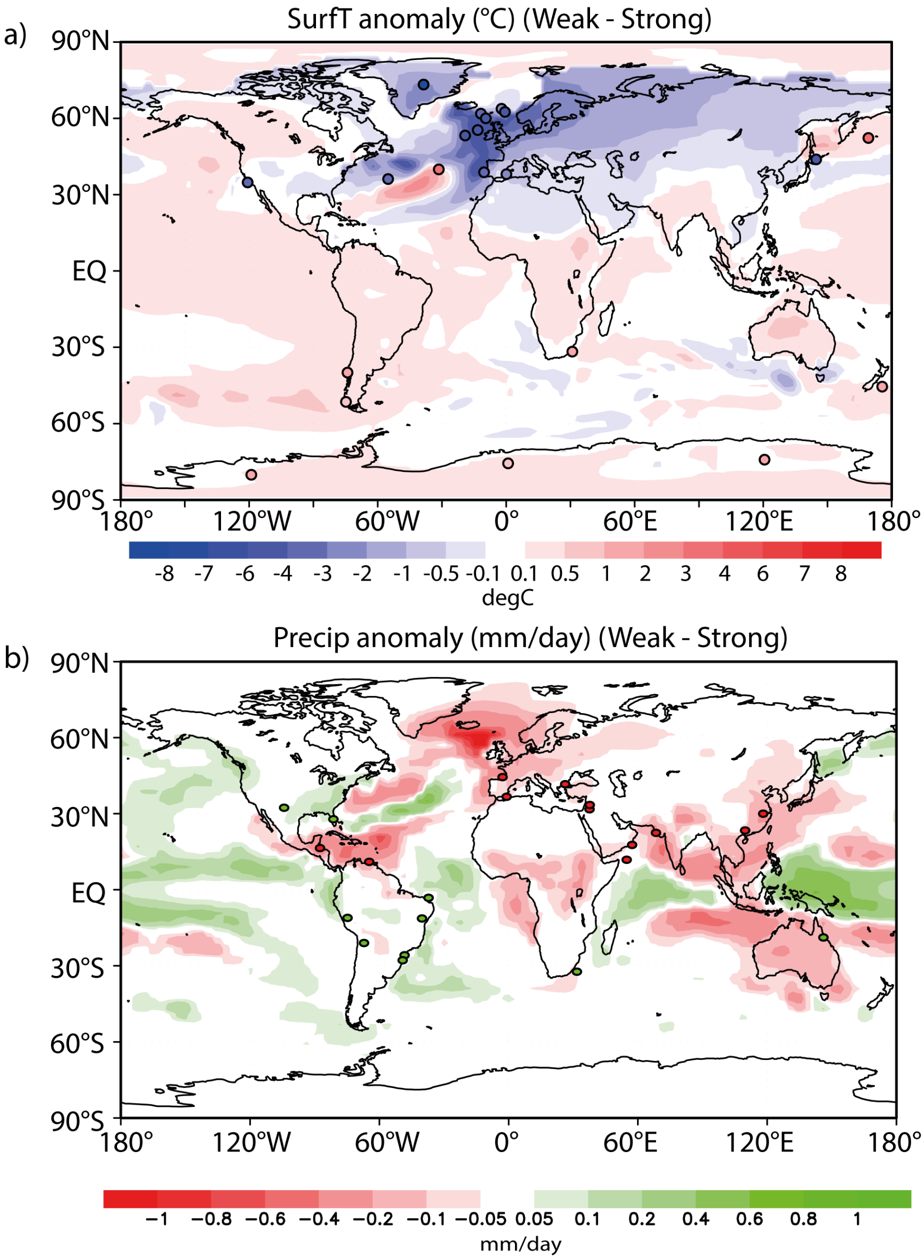

Figure S4 Simulated annual mean surface temperature and precipitation anomaly between the weak and strong AMOC modes with corresponding paleoclimate reconstructions. (a) Simulated surface air temperature and sea surface temperature (°C) anomaly (shaded) with reconstructed temperature changes (dots); **(b)** simulated precipitation (mm/day) anomaly with superimposed precipitation records (dots). The simulated climatology of the weak and strong AMOC modes is defined as time-mean of period BD' and B'D as prescribed in Figure 1a, respectively. In a), red and blue dots quantitatively represent warm and cold conditions, respectively, during cold stadials, as also shown in Table S2. In b), green and red dots qualitatively indicate humid and arid conditions, respectively, during cold stadials, as also shown in Table S3.

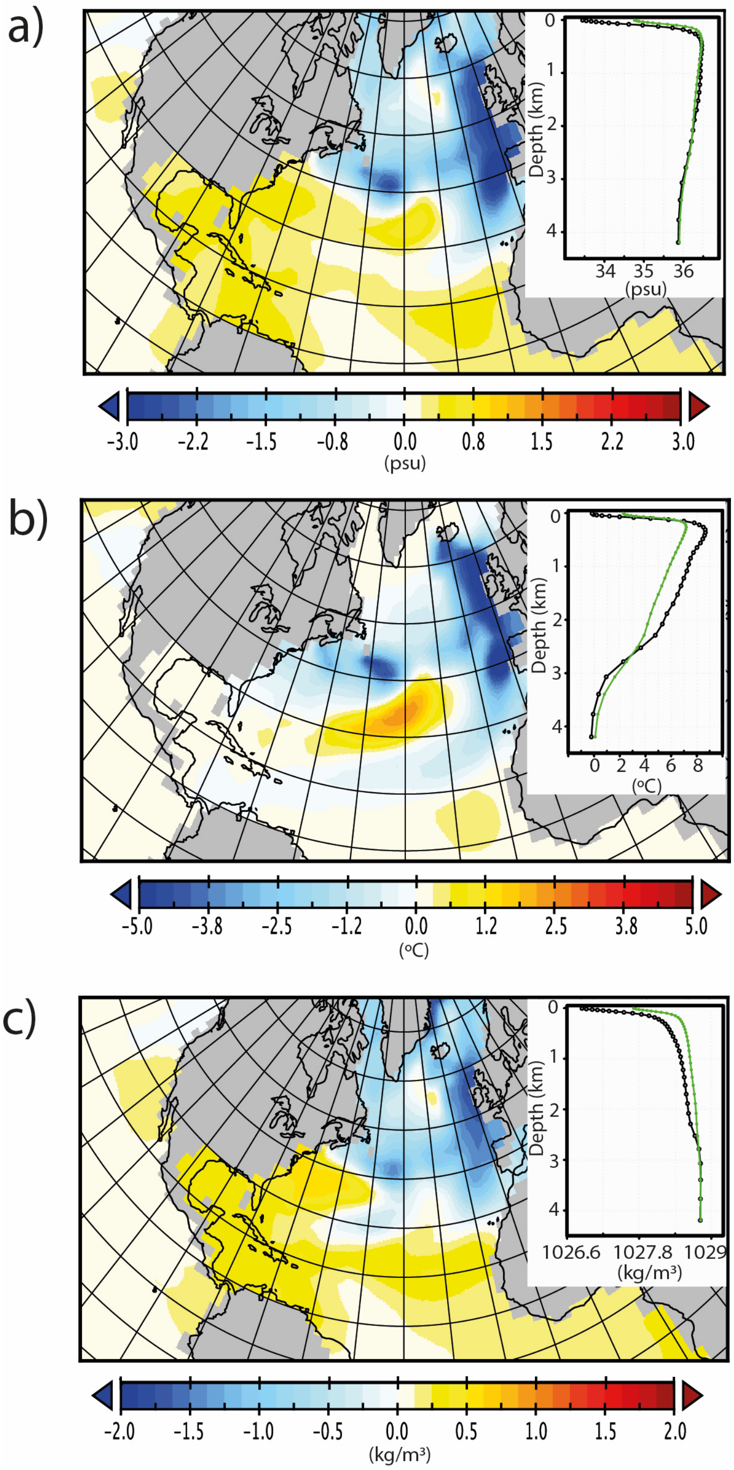

Figure S5 Same as Fig. S4, but for ocean properties. (a, b, c) Anomalies in simulated sea surface salinity (psu), temperature (°C) and density (kg/m^3), respectively. Vertical profiles in the NENA (50–65°N, 10–30°W) are shown in the up right corner of the corresponding spatial maps. In the profile plots, black and green curves represent absolute values in the weak and strong AMOC mode, respectively.

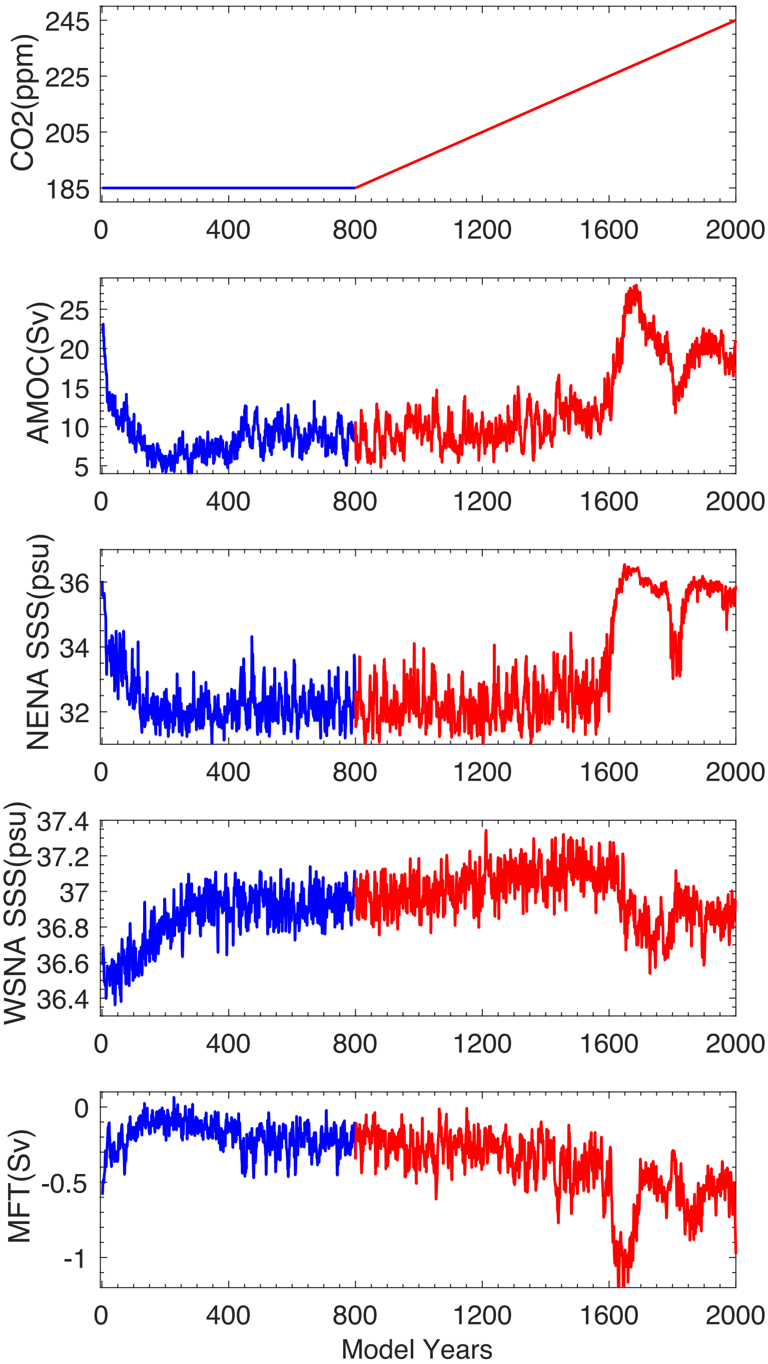

Figure S6 Changes in sea surface salinity (SSS) in experiment LGM_015 and LGM_015_CO2. (from up to bottom) CO_2 forcing (ppm), AMOC index (Sv), salinity in the NENA and WSNA, and meridional freshwater transport (Sv). The blue lines represent the control simulation LGM_015, and red lines indicate experiment LGM_015_CO2. Noted that the NA freshwater perturbation of 0.15Sv always exists in both experiments. x-axis represents model years (units: year).

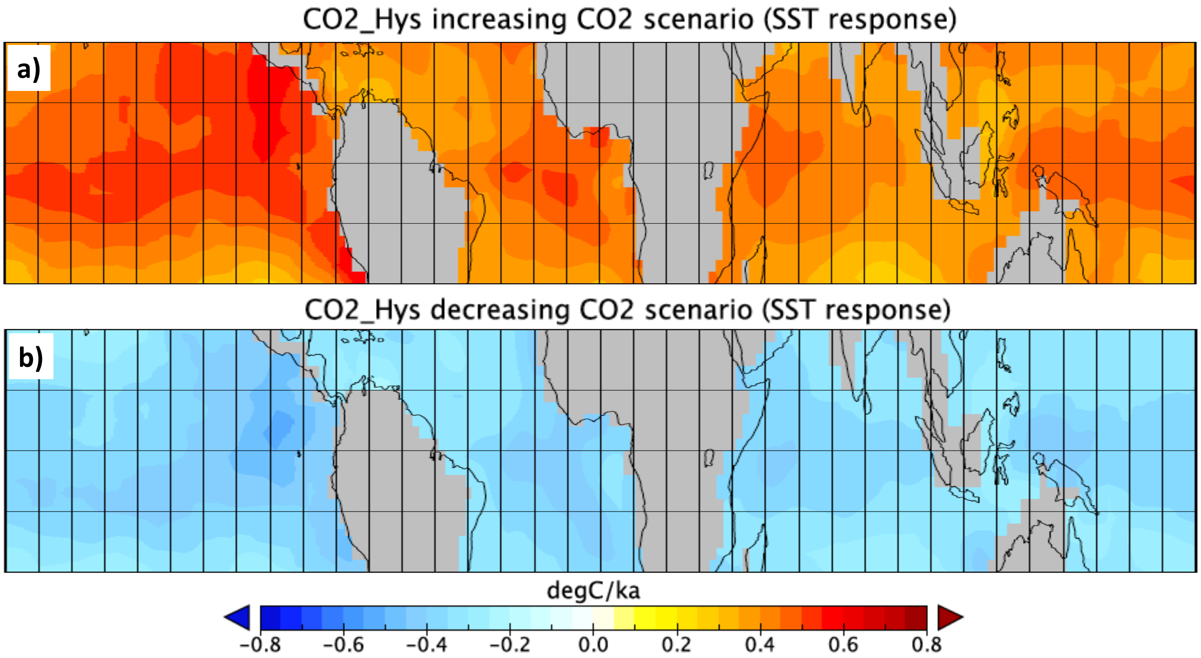

Figure S7 Responses of tropical sea surface temperature to CO_2 changes in experiment CO2_Hys. a) and **b)** are trend analysis of sea surface temperature in the CO_2 increasing (interval A-B in Fig. 1a) and decreasing scenarios (interval C-D in Fig. 1A). Units: °C/ka.

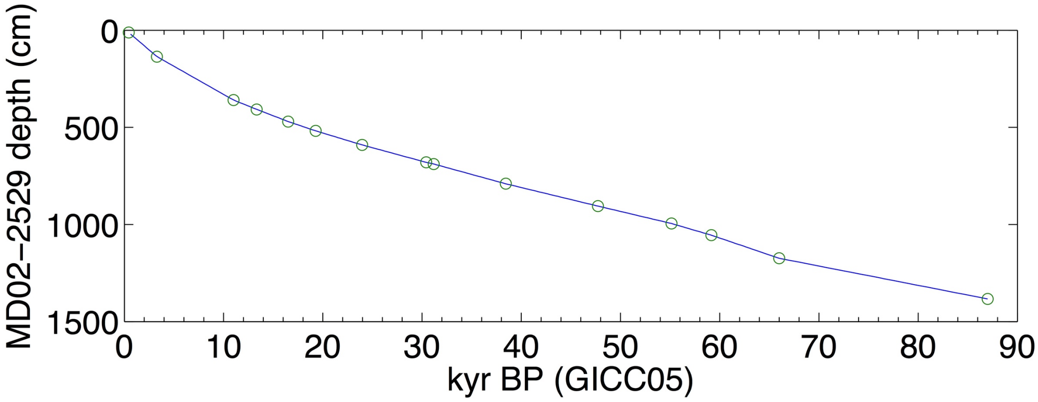

Figure S8 Depth-age relationship of core MD02-2529 in GICC05 chronology.

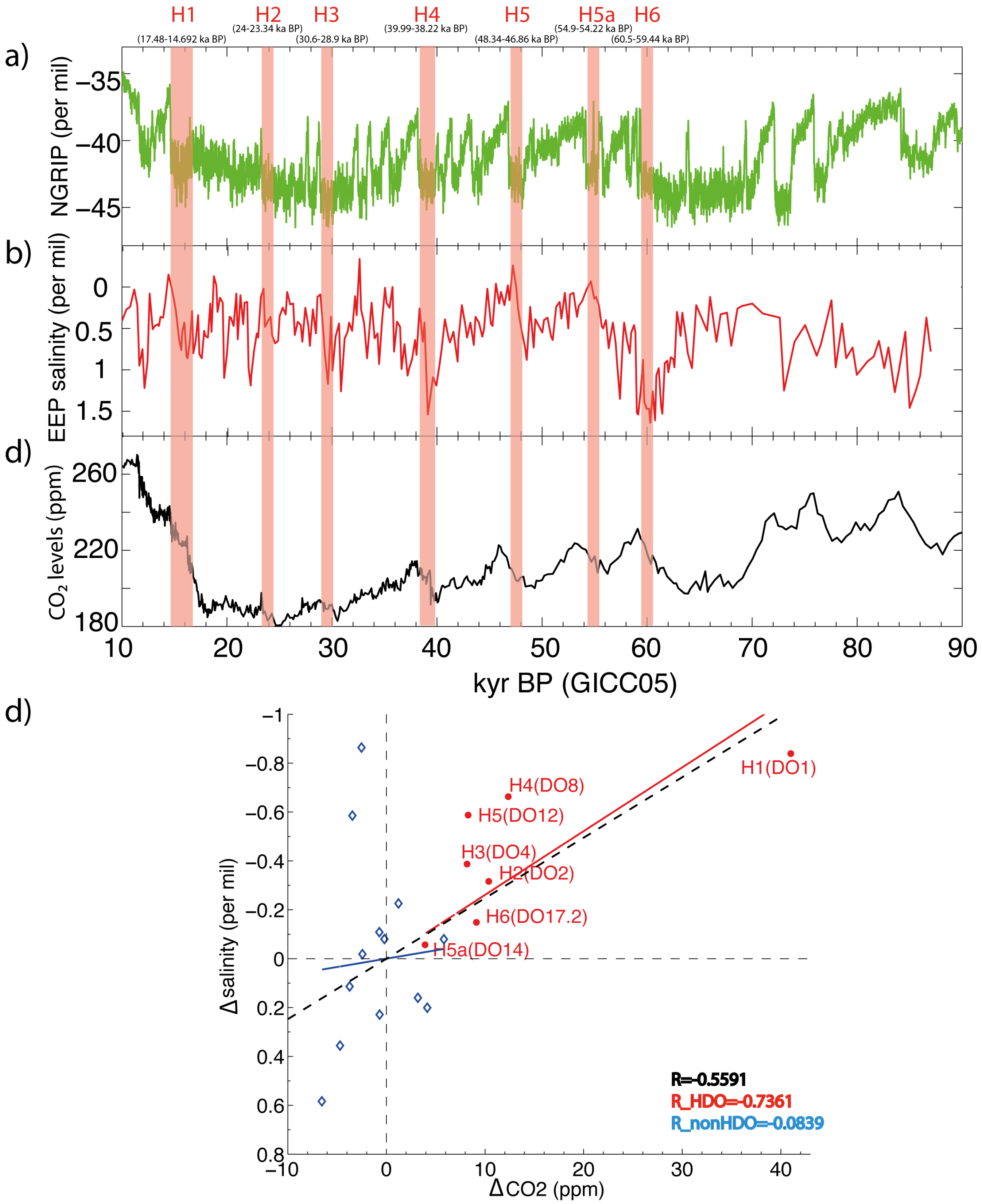

Figure S9 Climate records of the last glacial period. **(a)** The NGRIP records[56], **(b)** the EEP paleo-salinity[38] and **(c)** atmospheric CO_2 records[20] with the GICC05 age scale[57], and **(d)** reconstructed relationship between the EEP sea surface salinity[38] and atmospheric CO_2[20] during stadials of the last glacial period. In subplot d), the red dots indicate the Heinrich stadials that are also highlighted in (a-c) by red rectangle, while blue diamonds represent the non-Heinrich stadials. Red, blue and black dashed lines indicate the linear regression between changes in CO_2 and EEP salinity during Heinrich stadials (R_HDO), non-Heinrich stadials (R_nonHDO) and all stadials (R), respectively. The linear regression values are shown in the lower right corner of d). Negative Δsalinity represents salinity decrease. Definition of stadial intervals (on the top of Figure S9a) is mainly based on Rasmussen et al., [2014][58], and depth-age relation of the EEP salinity record with GICC05 age scale[57] is shown in Fig. S8.

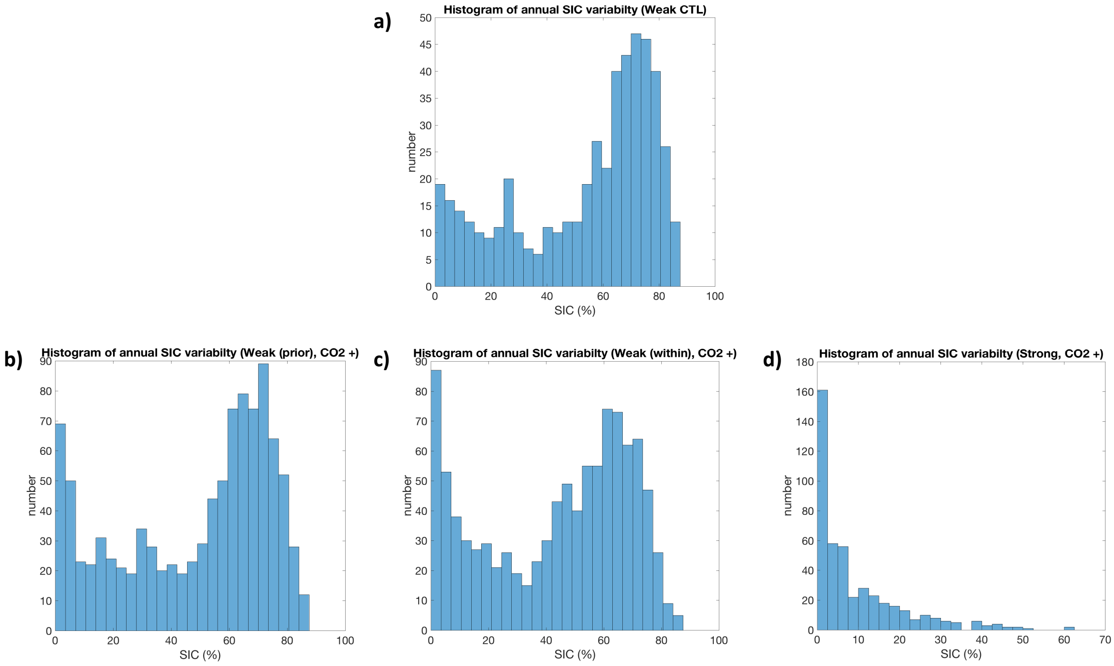

Figure S10 Histogram of sea ice variability in the North Atlantic (20-30°W, 56-62°N) under the CO_2 increasing scenario of CO2_Hys. a) is for control experiment LIS_0.2, **b**) for the interval *A-D'* of Fig 1a, c) for the interval *D'-B* of Fig 1a and d) for the 2100th-2750th model year of CO2_Hys. Please refer to Fig. S11c for climatology annual mean sea ice concentration in the weak AMOC mode.

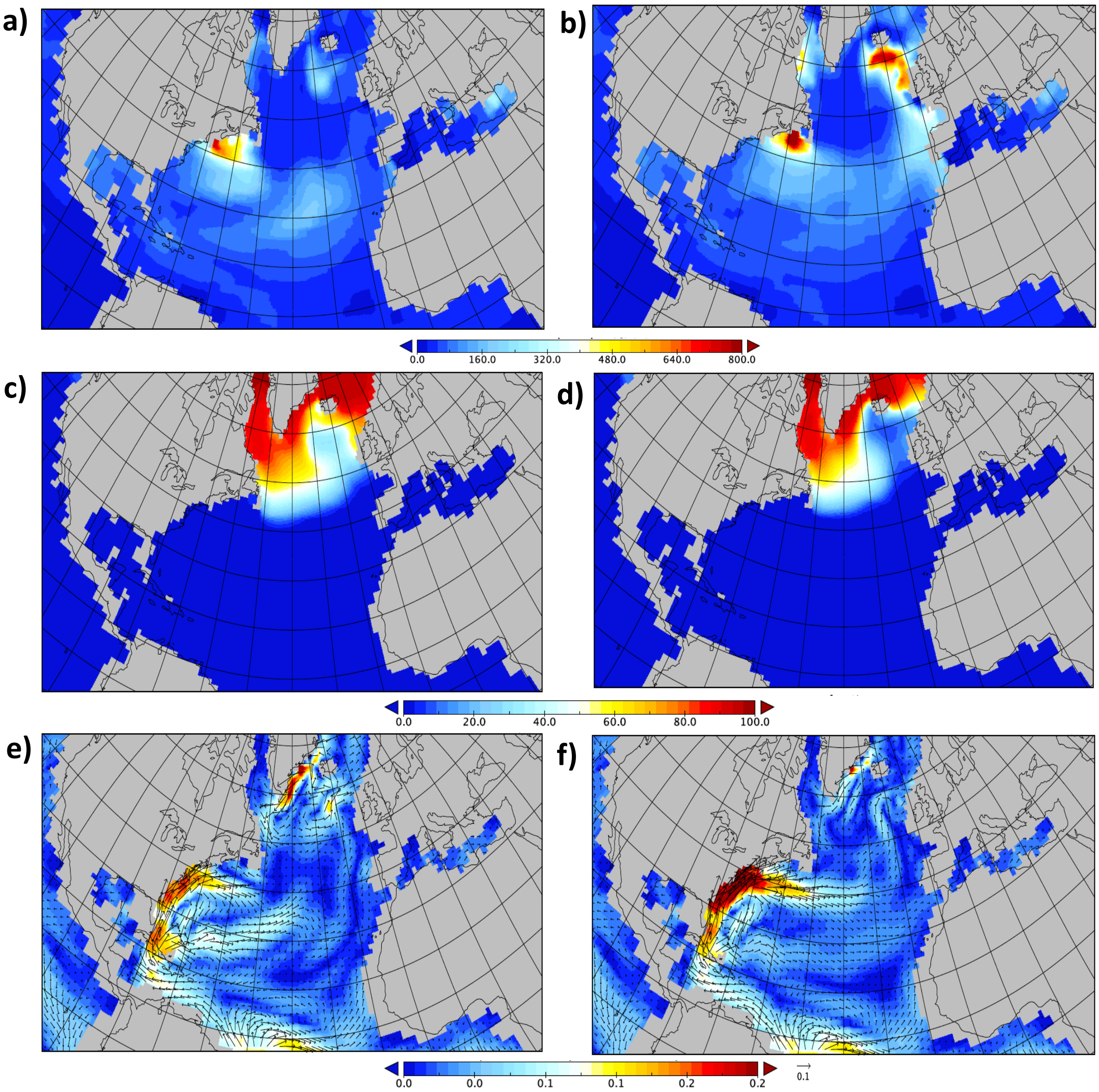

Figure S11 Climatology fields of the weak (a, c, e) and strong (b, d, f) AMOC modes in experiment CO2_Hys. a) and **b)** are mixed layer depth (units: m); **c)** and **d)** are sea ice concentration (units: percentage) and **e)** and **f)** are ocean currents (vectors) above 60m water depth, shaded for the magnitude (units: m/s). The simulated climatology of the weak and strong AMOC modes is defined as time-mean of period BD’ and B’D as prescribed in Figure 1a, respectively

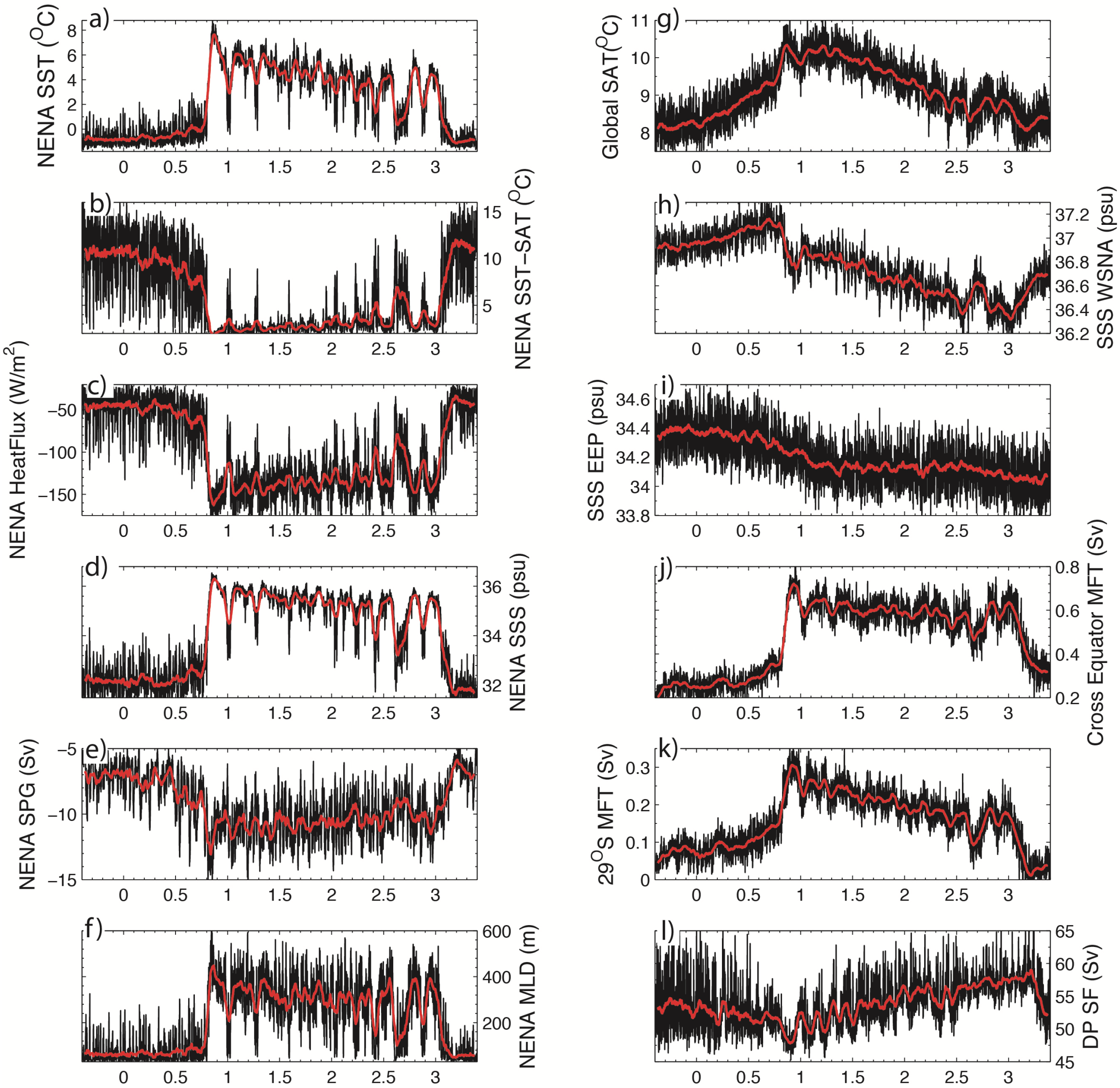

Figure S12 Time series of climate variables in LGM_0.15_CO2. Same as Fig. S2, but for the experiment LGM_0.15_CO2. X-axis represents model years (units: kyr)

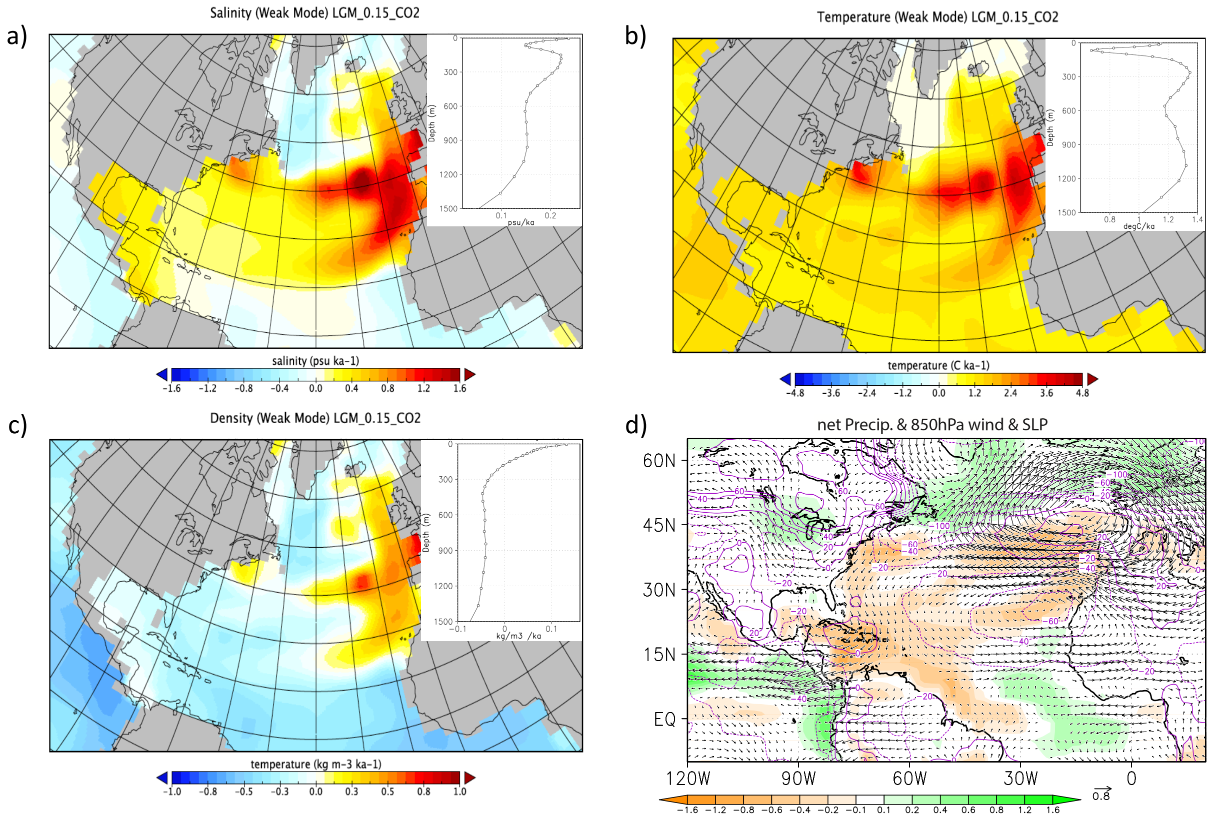

Figure S13 Trend analysis in the increasing CO_2 scenario of experiment LGM_0.15_CO2. (a, b, c) Trend of sea surface salinity (psu/ka), temperature (℃/ka) and density (kg/m^3/ka) and (d) trend of net precipitation (mm/day /ka, shaded), 850hPa wind (m/s /ka, vector), and sea level pressure trend (Pa/ka, contour) in the CO_2 increasing scenario (0-750th model year of experiment LGM_0.15_CO2 in Fig. 1h-n). The corresponding vertical profiles over the NENA (50–65 °N, 10–30 °W) are plotted in the upper right corner of the associated spatial maps in (a-c).

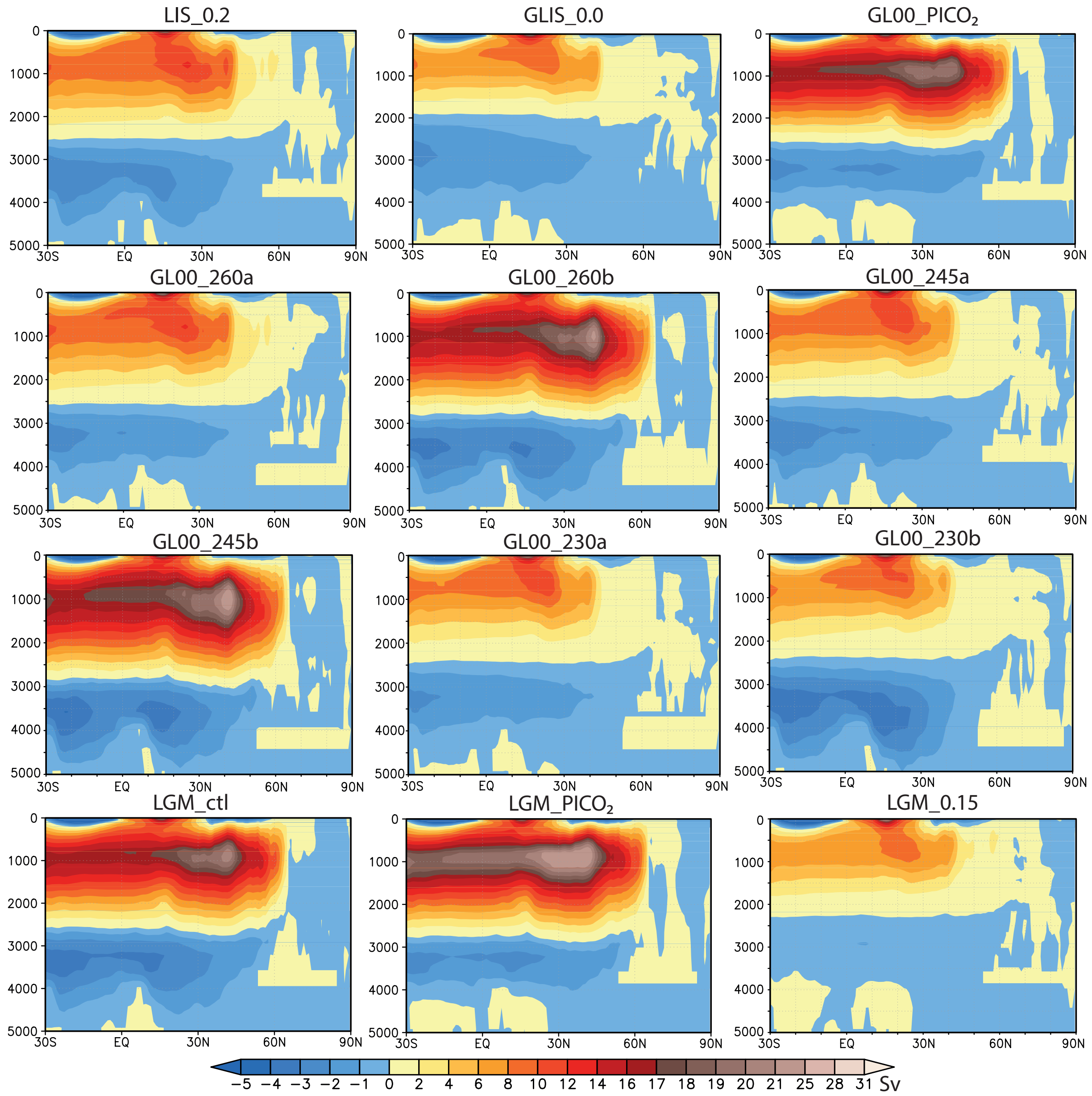

Figure S14 Spatial map of the AMOC under different climate scenarios. The last 100-year average is considered to represent the corresponding climatology. The detailed information of these experiments is shown in Table S1.

	ID	Initial Ocean State	e.s.l. (m)	CO_2 (ppm)	Other forcing	Integrated years
Equilibrium runs						
	NHIS_0.2	LGM	~42	185	LGM	600
	GLIS_0.0	LGM	0	185	LGM	2000
	GL00_230a	GLIS_0.0	0	230	LGM	2000
	GL00_245a	GL00_230a	0	245	LGM	1600
	GL00_260a	GL00_245a	0	260	LGM	1600
	GL00_PICO$_2$	GLIS_0.0	0	280	LGM	1000
	GL00_260b	GL00_PICO$_2$	0	260	LGM	1500
	GL00_245b	GL00_260b	0	245	LGM	1500
	GL00_230b	GL00_245b	0	230	LGM	1500
	LIS_0.2	NHIS_0.2	~42	185	LGM	5000
	LGM_ctl	Glacial Ocean	~116	185	LGM	4000
	LGM_PICO$_2$	LGM	~116	280	LGM	1100
	LGM_0.15	LGM	~116	185	LGM + 0.15Sv FWP in the NA	800
Transient runs						
	CO2_Hys	LIS_0.2	~42	<185~239> (0.02ppm/yr)	LGM	5400
	LGM_0.15_CO2	LGM_0.15	~116	<185~245> (0.05ppm/yr)	LGM + 0.15Sv FWP in the NA	2400

Table S1 Model simulations in this study. To qualify the impact of atmospheric CO_2 changes on glacial climate stability, other boundary conditions (ice sheet configuration, land sea mask, orbital parameters etc.) are always kept constant, if not specified. Experiment 'LGM_ctl' and Pre-industrial are LGM-W and PI runs in Zhang et al. [2013][9]. Experiment 'NHIS_0.2' is from Zhang et al. [2014][8]. The initial AMOC states in transient experiments are monostable with respect to the ice sheet configurations[8,9]. Specifically, the prescribed intermediate (maximum) level of the Northern Hemisphere ice sheets in experiment CO2_Hys (LGM_0.15_CO2) corresponds to a mono-stable ocean state with the weak (strong) AMOC mode.

Nr.	Core ID	Lat.	Lon.	Response to Stadials	Approximate Range (degC)	Proxy	Ref.
	Northern Hemisphere						
1	GISP2 ice core	72.6	-38.5	cooling	~8-16	ice core	Grootes et al. 1993; Huber et al. 2006[59,60]
2	ENAM93-21	62.73	-3.88	cooling	~1-3	planktic foraminifer assemblages	Rasmussen et al. 1996; Rasmussen and Thomsen 2008[61,62]
3	LINK 17	~61.3	-3	cooling	~2-5	planktic foraminifer assemblages	Rasmussen and Thomsen 2008[61]
4	ENAM 33	61.26	-11.12	cooling	~2-4	planktic foraminifer assemblages	Rasmussen et al. 2002; Rasmussen and Thomsen 2008[61,63]
5	DAPC-02	58.97	-9.62	cooling	~3-5	planktic foraminifer assemblages	Rasmussen et al., 2002; Rasmussen and Thomsen 2008[61,64]
6	ODP 980	55.43	-14.7	cooling	~4-6	planktic $\delta^{18}O$	McManus et al 1999[6]
7	M23414	53.53 7	-20.29	cooling	~3-5	planktic foraminifer diversities	Kandiano et al. 2004[65]
8	ODP 883	51.2	167.77	warming	~2.5-4	planktic foraminifer assemblages	Kiefer et al. 2001[66]
9	MD01-2412	44.53	145	cooling	~2-6	alkenone	Harada et al. 2006[67]
10	IODP U1313	41	-33	warming	~2-4	alkenone	Naafs et al. 2013[68]
11	MD01-2444	37.6	-10.13	cooling	~2-5	alkenone	Martrat et al. 2007[69]
12	MD95-2043	36.15	-2.62	cooling	~1-3	alkenone/pollen	Cacho et al. 1999[70]
13	ODP 893a	34.29	-120.37	cooling	~3-5	planktic foraminifer assemblages	Hendy and Kennett 2000[71]
14	MD95-2036	33.69	-57.57	cooling	~2-5	alkenone	Sachs and Lehmen 1999[72]
	Southern Hemisphere						
15	CD154 17-17k	-33.32	29.47	warming	~2	planktic foraminifer Mg/Ca	Simon et al., 2013[73]
16	ODP Site 1233	-41	-74.45	warming	~2-3	alkenone	Lamy et al 2004[74]
17	MD97-2120	-45.53	174.93	warming	~2-3	planktic foraminifer Mg/Ca	Pahnke et al 2003[75]
18	MD07-3128	-52.66	-75.57	warming	~1-2	alkenone	Caniupan et al 2011[76]
19	EDML ice core	-75	0	warming	~0.5-3	ice core	EPICA member 2006[77]
20	Dome C ice core	-75.06	123	warming	~1-3	ice core	EPICA member 2004[78]
21	Byrd ice core	-80	-129	warming	~1-3	ice core	Blunier and Brook, 2001[79]

Table S2 Temperature proxy data used for model-data comparison. Listed is the information regarding 21 temperature proxy records covering the period when atmospheric CO_2 is at varying intermediate levels (i.e. MIS3). Approximate range represents magnitudes of recorded temperature changes during cold stadials, as documented in the corresponding literature. In this study, we use the intermediate level of reconstructed amplitudes for the model-data comparison (as shown in Fig. S4a). For instance, if the proxy-recorded temperature fluctuation ranges between ~1-3 °C, we consider in our model-data comparison a conservative estimate of the reconstructed temperature fluctuation of ~2 °C.

Nr.	Core ID	Lat.	Lon.	Response to Cold Stadials	Proxy	Ref.
22	MD01-2348	~44	~5	arid	Pollen	Van Meerbeeck et al. 2011[80]
23	Tenaghi Philippon core	40.97	24.22	arid	Terrestrial archive	Mueller et al. 2011[81]
24	Fort Stanton stalagmite	33.3	-105.3	humid	Speleothem calcite $\delta^{18}O$	Asmerom et al. 2010[82]
25	Hulu Cave	32.5	119.17	arid	Stalagmite $\delta^{18}O$	Wang et al., 2001[83]
26	Peqiin Cave	32.58	35.19	arid	Cave speleothem $\delta^{18}O$	Bar-Matthews et al., 2003[84]
27	Soreq Cave	31.45	35.03	arid	Cave speleothem $\delta^{18}O$	Bar-Matthews et al., 2003[84]
28	Lake Tulane NAD27	27.59	-81.5	humid	Pollen and plant macrofossils	Grimm et al. 2006[85]
29	Dongge Cave	25.28	108.08	arid	Stalagmite $\delta^{18}O$	Yuan et al., 2004[86]
30	SO90-111KL/SO90-136KL	23.1	66.48	arid	Total organic carbon	Schulz et al. 1998[87]
31	RC27-23/RC27-14	18	57.65	arid	$\delta^{15}N$	Altabet et al. 2002[88]
32	Lake Peten Itza	16.92	-89.83	arid	Clay-gypsum	Hodell et al. 2008[89]
33	Socatra Island	12.5	54	arid	Stalagmite $\delta^{18}O$	Burns et al. 2003[90]
34	ODP hole 1002C	10.71	-65.17	arid	Ti/Fe ratio	Peterson et al. 2000[28]
35	GeoB3104-1/GeoB3912-1	-3.67	-37.72	humid	Fe/Ca ratio	Jennerjahn et al. 2004[91]
36	Northeastern Brazilian calcite speleothems	-10.17	-40.83	humid	Speleothem and travertine deposit	Wang et al. 2004[92]
37	Pacupahuain Cave Stalagmite P09-PH2	-11.24	-75.82	humid	Speleothem calcite $\delta^{18}O$	Kanner et al. 2012[93]
38	Lynch's crater	-17.62	146.17	humid	Degree of peat humification and ratio of sedges to grass	Turney et al. 2004[94]
39	Salar de Uyuni core	-20.23	-67.5	humid	Natural r-rays	Baker et al. 2001[95]
40	Santana Cave Stalagmite St8	-24.53	-48.73	humid	Speleothem calcite $\delta^{18}O$	Cruz et al. 2006[96]
41	Caverna Botuvera Stalegmites	-27.22	-49.15	humid	Speleothem calcite $\delta^{18}O$	Wang et al., 2006[97]
42	Botuvera Cave Stalagmite Bt2	-27.22	-49.16	humid	Stalagmite $\delta^{18}O$	Cruz et al. 2005[98]
43	CD 154-17-17k	-33.27	29.12	humid	Fe/K ratio	Ziegler et al., 2013[99]

Table S3 Information regarding 22 reconstructed precipitation records used for model-data comparison. The records covering the period when atmospheric CO_2 is at varying intermediate levels (i.e. MIS3). Qualitatively reconstructed precipitation records are used to compare with simulated precipitation anomalies between the weak and strong AMOC modes as shown in Fig. S4b.

References:

54. Toggweiler, J. R. & Russell, J. Ocean circulation in a warming climate. *Nature* **451,** 286–288 (2008).

55. Zaucker, F. & Broecker, W. S. The Influence of Atmospheric Moisture Transport on the Fresh Water Balance of the Atlantic Drainage Basin: General Circulation Model Simulations and Observations. *J. Geophys. Res.* **97,** 2765–2773 (1992).

56. Seierstad, I. K. *et al.* Consistently dated records from the Greenland GRIP, GISP2 and NGRIP ice cores for the past 104 ka reveal regional millennial-scale δ18O gradients with possible Heinrich event imprint. *Quat. Sci. Rev.* **106,** 29–46 (2014).

57. Wolff, E. W., Chappellaz, J., Blunier, T., Rasmussen, S. O. & Svensson, a. Millennial-scale variability during the last glacial: The ice core record. *Quat. Sci. Rev.* **29,** 2828–2838 (2010).

58. Rasmussen, S. O. *et al.* A stratigraphic framework for abrupt climatic changes during the Last Glacial period based on three synchronized Greenland ice-core records: refining and extending the INTIMATE event stratigraphy. *Quat. Sci. Rev.* **106,** 14–28 (2014).

59. Grootes, P. M., Stulver, M., White, J. W. C., Johnsen, S. & Jouzel, J. Comparison of Oxygen isotope records from the GISP2 and GRIP Greenland ice cores. *Nature* **366,** 552–554 (1993).

60. Huber, C. *et al.* Isotope calibrated Greenland temperature record over Marine Isotope Stage 3 and its relation to CH4. *Earth Planet. Sci. Lett.* **243,** 504–519 (2006).

61. Rasmussen, T. L. & Thomsen, E. Warm Atlantic surface water inflow to the Nordic seas 34-10 calibrated ka B.P. *Paleoceanography* **23,** PA1201 (2008).

62. Rasmussen, T. & Thomsen, E. Circulation changes in the Faeroe-Shetland Channel correlating with cold events during the last glacial period (58–10 ka). *Geology* **24,** 937–940 (1996).

63. Rasmussen, T., Thomsen, E., Troelstra, S. R., Kuijpers, A. & Prins, M. a. Millennial-

scale glacial variability versus Holocene stability: changes in planktic and benthic foraminifera faunas and ocean circulation in the North Atlantic during the last 60 000 years. *Mar. Micropaleontol.* **47,** 143–176 (2002).

64. Rasmussen, T. L. *et al.* The Faroe-Shetland Gateway : Late Quaternary water mass exchange between the Nordic seas and the northeastern Atlantic. *Mar. Geol.* **188,** 165–192 (2002).

65. Kandiano, E. S., Bauch, H. a. & Müller, a. Sea surface temperature variability in the North Atlantic during the last two glacial–interglacial cycles: comparison of faunal, oxygen isotopic, and Mg/Ca-derived records. *Palaeogeogr. Palaeoclimatol. Palaeoecol.* **204,** 145–164 (2004).

66. Kiefer, T., Sarnthein, M., Erlenkeuser, H., Grootes, P. M. & Roberts, A. P. North Pacific response to millennial-scale changes in ocean circulation over the last 60 kyr. *Paleoceanography* **16,** 179–189 (2001).

67. Harada, N. *et al.* Rapid fluctuation of alkenone temperature in the southwestern Okhotsk Sea during the past 120 ky. *Glob. Planet. Change* **53,** 29–46 (2006).

68. Naafs, B. D. A., Hefter, J., Grützner, J. & Stein, R. Warming of surface waters in the mid-latitude North Atlantic during Heinrich events. *Paleoceanography* **28,** 153–163 (2013).

69. Martrat, B. *et al.* Four Climate Cycles of Recurring Deep and Surface Water Destabilizations on the Iberian Margin. *Science* **317,** 502–507 (2007).

70. Cacho, I., Grimalt, J. & Pelejero, C. Dansgaard-Oeschger and Heinrich event imprints in Alboran Sea paleotemperatures. *Paleoceanography* **14,** 698–705 (1999).

71. Hendy, I. & Kennett, J. Dansgaard-Oeschger cycles and the California Current System: Planktonic foraminiferal response to rapid climate change in Santa Barbara Basin , Ocean Drilling Program hole 893A. *Paleoceanography* **15,** 30–42 (2000).

72. Sachs, J. P. & Lehmann, S. J. Subtropical North Atlantic Temperatures 60,000 to 30,000

Years Ago. *Science* **286,** 756–759 (1999).

73. Simon, M. H. *et al.* Millennial-scale Agulhas Current variability and its implications for salt-leakage through the Indian–Atlantic Ocean Gateway. *Earth Planet. Sci. Lett.* **383,** 101–112 (2013).

74. Lamy, F. *et al.* Antarctic timing of surface water changes off Chile and Patagonian ice sheet response. *Science* **304,** 1959–1962 (2004).

75. Pahnke, K., Zahn, R., Elderfield, H. & Schulz, M. 340000 year Centennial-scale Marine Record of Southern Hemisphere Climatic Oscillation. *Science* **301,** 948–952 (2003).

76. Caniupán, M. *et al.* Millennial-scale sea surface temperature and Patagonian Ice Sheet changes off southernmost Chile (53°S) over the past ~60 kyr. *Paleoceanography* **26,** PA3221 (2011).

77. Barbante, C. *et al.* One-to-one coupling of glacial climate variability in Greenland and Antarctica. *Nature* **444,** 195–198 (2006).

78. Augustin, L. *et al.* Eight glacial cycles from an Antarctic ice core. *Nature* **429,** 623–628 (2004).

79. Blunier, T. & Brook, E. J. Timing of millennial-scale climate change in Antarctica and Greenland during the last glacial period. *Science* **291,** 109–112 (2001).

80. Van Meerbeeck, C. J. *et al.* The nature of MIS 3 stadial–interstadial transitions in Europe: New insights from model–data comparisons. *Quat. Sci. Rev.* **30,** 3618–3637 (2011).

81. Müller, U. C. *et al.* The role of climate in the spread of modern humans into Europe. *Quat. Sci. Rev.* **30,** 273–279 (2011).

82. Asmerom, Y., Polyak, V. J. & Burns, S. J. Variable winter moisture in the southwestern United States linked to rapid glacial climate shifts. *Nat. Geosci.* **3,** 114–117 (2010).

83. Wang, Y. J. *et al.* A high-resolution absolute-dated late Pleistocene Monsoon record from Hulu Cave, China. *Science* **294,** 2345–2348 (2001).

84. Bar-Matthews, M., Ayalon, A., Gilmour, M., Matthews, A. & J., H. C. Sea–land oxygen isotopic relationships from planktonic foraminifera and speleothems in the Eastern Mediterranean region and their implication for paleorainfall during interglacial intervals. *Geochim. Cosmochim. Acta* **67,** 3181–3199 (2003).

85. Grimm, E. C. *et al.* Evidence for warm wet Heinrich events in Florida. *Quat. Sci. Rev.* **25,** 2197–2211 (2006).

86. Yuan, D. *et al.* Timing, duration, and transitions of the last interglacial Asian monsoon. *Science* **304,** 575–578 (2004).

87. Schulz, H., Rad, U. von & Erlenkeuser, H. Correlation between Arabian Sea and Greenland climate oscillations of the past 110,000 years. *Nature* **393,** 23–25 (1998).

88. Altabet, M., Higginson, M. & Murray, D. The effect of millennial-scale changes in Arabian Sea denitrication on atmospheric CO2. *Nature* **764,** 159–162 (2002).

89. Hodell, D. a. *et al.* An 85-ka record of climate change in lowland Central America. *Quat. Sci. Rev.* **27,** 1152–1165 (2008).

90. Burns, S. J., Fleitmann, D., Matter, A., Kramers, J. & Al-Subbary, A. a. Indian Ocean climate and an absolute chronology over Dansgaard/Oeschger events 9 to 13. *Science* **301,** 1365–1367 (2003).

91. Jennerjahn, T. C. *et al.* Asynchronous terrestrial and marine signals of climate change during Heinrich events. *Science* **306,** 2236–2239 (2004).

92. Wang, X. *et al.* Wet periods in northeastern Brazil over the past 210 kyr linked to distant climate anomalies. *Nature* **432,** 740–743 (2004).

93. Kanner, L. C., Burns, S. J., Cheng, H. & Edwards, R. L. High-latitude forcing of the South American summer monsoon during the Last Glacial. *Science* **335,** 570–573 (2012).

94. Turney, C., Kershaw, A. & Clemens, S. Millennial and orbital variations of El Nino/Southern Oscillation and high-latitude climate in the last glacial period. *Nature*

428, 306–310 (2004).

95. Baker, P. A *et al.* Tropical climate changes at millennial and orbital timescales on the Bolivian Altiplano. *Nature* **409,** 698–701 (2001).

96. Cruz, F. W., Burns, S. J., Karmann, I., Sharp, W. D. & Vuille, M. Reconstruction of regional atmospheric circulation features during the late Pleistocene in subtropical Brazil from oxygen isotope composition of speleothems. *Earth Planet. Sci. Lett.* **248,** 495–507 (2006).

97. Wang, X. *et al.* Interhemispheric anti-phasing of rainfall during the last glacial period. *Quat. Sci. Rev.* **25,** 3391–3403 (2006).

98. Cruz Jr, F. W. *et al.* Insolation-driven changes in atmospheric circulation over the last 116000 years in subtropical Brazil. *Nature* **434,** 63–66 (2005).

99. Ziegler, M. *et al.* Development of Middle Stone Age innovation linked to rapid climate change. *Nat. Commun.* **4,** 1905 (2013).